Color-Image Quality Assessment: From Prediction to Optimization

Jens Preiss, Felipe Fernandes, and Philipp Urban

***Abstract*— While image-difference metrics show good prediction performance on visual data, they often yield artifact-contaminated results if used as objective functions for optimizing complex image-processing tasks. We investigate in this regard the recently proposed color-image-difference (CID) metric particularly developed for predicting gamut-mapping distortions. We present an algorithm for optimizing gamut mapping employing the CID metric as the objective function. Resulting images contain various visual artifacts, which are addressed by multiple modifications yielding the improved color-image-difference (iCID) metric. The iCID-based optimizations are free from artifacts and retain contrast, structure, and color of the original image to a great extent. Furthermore, the prediction performance on visual data is improved by the modifications.**

***Index Terms*— Image difference, image quality, color, gamut mapping.**

I. Introduction

HIGHER order cortical mechanisms of the human visual system (HVS) are only poorly understood so far [1]. For the complex task of assessing perceived image quality, many approaches, therefore, rely on hypothesis to which image distortions the HVS is particularly sensitive [2]. When a reference image is available, the quality of a distorted image is described by a metric[1] that predicts the perceived difference between the two images – a so-called Image-Difference Metric (IDM). For some distortions, such as JPEG compression, noise, and blur, predictions of today's IDMs correlate remarkably well with human perception [3]. For other distortions, such as those resulting from gamut mapping or tone mapping, there is still much room for improvement [4].

To evaluate how well IDM predictions agree with human perception, rank-order correlation (e.g., Spearman [5] or Kandell [6]) or the hit rate (see Section IV-B) may be used. These figures of merit are employed to optimize or compare IDMs on visual data containing psychophysically evaluated distortions between images. Adjusting IDMs on such data is, however, problematic, particularly if the distortions are caused by complex image-processing algorithms such as gamut mapping or tone mapping. In these cases, resulting IDMs are inherently biased by heuristics employed by the underlying image-processing algorithm. One example is gamut mapping where the vast majority of algorithms preserve hue [7]. The impact of hue deviations on perceived image differences cannot be meaningfully extracted from such data.

To be less dependent on heuristics used by distortion operators and thus included in visual data, we need to change the strategy to optimize IDMs. For this, we need to look onto general properties an IDM has to satisfy. The most important property of an IDM $\mathbf{d}$ is its agreement with the population-average image-difference perception $\mathbf{v}$, i.e., $\forall X, Y, Z \in \mathbb{E}$:

$$\mathbf{v}(X, Y) \leq \mathbf{v}(X, Z) \Leftrightarrow \mathbf{d}(X, Y) \leq \mathbf{d}(X, Z), \tag{1}$$

where $\mathbb{E}$ is the set of all equally sized images. In other words: the metric mimics the decisions of the population-average observer in a paired-comparison experiment for arbitrary images X, Y, Z.

Based on the importance of this property, Wang et al. [8] proposed a "more efficient methodology for examining the relationship between [...] objective measure and perceived quality", which is "an expedient and direct method for revealing perceptual implications of the quality measure". Given a distorted image, they used the IDM as an objective function to minimize/maximize its difference to the reference image preserving the initial mean squared error (MSE). The resulting images of both optimizations have a similar MSE to the reference and are the best and worst case images indicating the types of distortions deemed to be least/most important by the IDM.

In this paper, we adapt the optimization approach for improving the prediction performance of a color IDM particularly dedicated to gamut-mapping distortions. The so-called Color-Image-Difference (CID) metric [9] is a color extension of the SSIM index [8]. It correlates significantly better with human judgments on a large visual database containing gamut-mapping distortions than all twelve quality metrics provided by the MeTriX MuX package [10] (including SSIM [8], MSSIM [11], and VIF [12]).

In a conference paper [13], gamut mapping was recently introduced as a constrained optimization problem with the CID metric as an objective function. Results revealed that the optimized images show a significantly smaller disagreement to the original images than results from common

Manuscript received May 24, 2013; revised October 3, 2013 and December 20, 2013; accepted January 14, 2014. Date of publication January 27, 2014; date of current version February 18, 2014. This work was supported by the German Research Foundation. The associate editor coordinating the review of this manuscript and approving it for publication was Prof. Sanghoon Lee.

J. Preiss and F. Fernandes are with the Institute of Printing Science and Technology, Technische Universität Darmstadt, Darmstadt 64289, Germany (e-mail: preiss@idd.tu-darmstadt.de; fernandes@idd.tu-darmstadt.de).

P. Urban is with the Fraunhofer Institute for Computer Graphics Research IGD, Darmstadt 64283, Germany (e-mail: philipp.urban@igd.fraunhofer.de).

Color versions of one or more of the figures in this paper are available online at http://ieeexplore.ieee.org.

Digital Object Identifier 10.1109/TIP.2014.2302684

[1]Please note that the term *metric* is used in the image-quality-assessment community even though mathematical metric properties might be violated.

gamut-mapping algorithms. However, optimized images were not free from artifacts indicating that improvements on the CID metric are likely.

We show in this paper how to modify the CID metric to avoid artifacts in the optimization process. As a byproduct, we obtain a gamut-mapping algorithm that minimizes both the predicted and the perceived difference between gamut-mapped and original image.

II. Gamut Mapping as a Constrained Optimization Problem

The set of colors reproducible by a particular device, the *device gamut*, is limited. *Gamut mapping* refers to the process of reproducing colors that exceed the limitations of the device. Morovič [7] gives a good overview of this topic. A common objective of gamut-mapping methods is to minimize the perceived difference between the gamut-mapped and the original image. Almost all approaches incorporate assumptions to which image distortions the human visual system is particularly sensitive and try to alter the image avoiding such distortions. Hue shifts, for instance, are particularly disturbing because they affect memory colors (e.g., brand or skin colors) [14]. Therefore, many gamut-mapping methods preserve hue [7]. Another example of highly disturbing distortions are banding artifacts or the loss of local structure. For retaining local color contrasts, a new class of approaches called *spatial gamut-mapping algorithms* was developed [15]–[18].

To perform optimally, gamut-mapping methods must balance the impact of possible distortions according to their perceptual importance. A dual problem is the formulation of gamut mapping as a constrained optimization problem employing an IDM $\mathbf{d}$ that correlates well with image-difference perception as the objective function:

$$Z = \underset{Y \widetilde{\subset} \mathbf{G}}{\operatorname{argmin}} \, \mathbf{d}(X, Y), \tag{2}$$

where X is the original and Z the gamut-mapped image and the expression $Y \widetilde{\subset} \mathbf{G}$ means that all colors of Y are within the gamut $\mathbf{G}$.

Only little work was published so far addressing this problem. Nakauchi et al. [19] used a metric similar to S-CIELAB as an objective function. S-CIELAB shows, however, poor correlation with visual data obtained in gamut-mapping experiments [4]. Kimmel et al. [20] used a related metric but included a gradient difference to preserve local contrast variations. The resulting gamut-mapped images were not free from halo artifacts which required modifications of the objective function especially along strong edges. Alsam and Farup [21] proposed a related approach based on anisotropic diffusion being able to strongly reduce the halo artifacts. Zolliker et al. [22] employed a hue-enhanced version of the SSIM index to fuse images already gamut-mapped by multiple algorithms. In the fusion process the original image is separated in regions and the enhanced SSIM index chooses the best rated algorithm for each region. In visual experiments, fused images were judged to be more similar to the original than each of the images used for the fusing process. Please note that each fusion method is limited by the (local) quality of the input images.

A. Color-Image-Difference (CID) Metric

To solve problem (2) the CID metric (see Appendix A) was used as the objective function for a gamut-mapping optimization [13]. It contains local comparison terms for computing lightness-difference l_L, lightness-contrast c_L, lightness-structure s_L, chroma-difference l_C, and hue-difference l_H as described in Appendix A (see Equations (16)–(20)). CID combines these terms as follows:

$$\mathbf{CID}_A(X, Y) = 1 - \frac{1}{|A|} \sum_{i \in A} \big[l_L(\mathbf{x}_i, \mathbf{y}_i) \cdot c_L(\mathbf{x}_i, \mathbf{y}_i) \cdot s_L(\mathbf{x}_i, \mathbf{y}_i) \cdot l_C(\mathbf{x}_i, \mathbf{y}_i) \cdot l_H(\mathbf{x}_i, \mathbf{y}_i) \big], \tag{3}$$

where $A \subseteq \Omega = \{1, \ldots, M\} \times \{1, \ldots, N\}$ is an index set with pixel positions of an image with M rows and N columns, $|A|$ is the number of elements of the index set, and $\mathbf{x}_i$ and $\mathbf{y}_i$ are defined equally as in Equation (15) (see Appendix A) assuming that an initial image-appearance-model transformation $\mathbf{N}$ was applied to the input images X and Y. Employing an index set A allows a convenient specification of image differences for subimages. To compute the overall color-image difference between both images, A must contain all pixel positions, i.e., $A = \Omega$.

B. Optimizing Gamut Mapping by the CID Metric

If image-appearance normalizations are not considered, the CID metric possesses the following property

$$(\mathbf{CID}_\Omega(X, Y + D_i) - \mathbf{CID}_\Omega(X, Y))|\Omega| = (\mathbf{CID}_W(X, Y + D_i) - \mathbf{CID}_W(X, Y))|W|, \tag{4}$$

where $\Omega = \{1, \ldots, M\} \times \{1, \ldots, N\}$, $i \in \Omega$ is a pixel position, W is a $k \times k$-window centered at i, and D_i is an image with $D_i(i) \in \mathbb{R}^3$ and $D_i(j) = (0, 0, 0)^T$ for all $j \neq i$, i.e., $Y + D_i$ changes only the pixel value at position i of image Y.

Since $\mathbf{CID}_A \geq 0$, $\forall A \subseteq \Omega$, the following implication can be derived from property (4):

$$\begin{aligned} &\mathbf{CID}_W(X, Y + D_i) \leq \mathbf{CID}_W(X, Y) \\ &\Rightarrow \mathbf{CID}_\Omega(X, Y + D_i) \leq \mathbf{CID}_\Omega(X, Y). \end{aligned} \tag{5}$$

This property of the CID metric allows to derive a descent direction for the gamut-mapping optimization by considering only pixels within a small window. The continuous optimization problem is turned into a discrete one by quantizing the pixels' domain color space. For this purpose, the nearly perceptually uniform LAB2000HL color space [23] was subdivided into equally-sized cubes, each representing one color in the quantized space. If a small fraction of the just-noticeable difference (JND) is used as the cubes' side length ϵ_{JND}, adjacent colors within the quantized LAB2000HL space are indistinguishable. In the following, this space is the domain of all pixel colors.

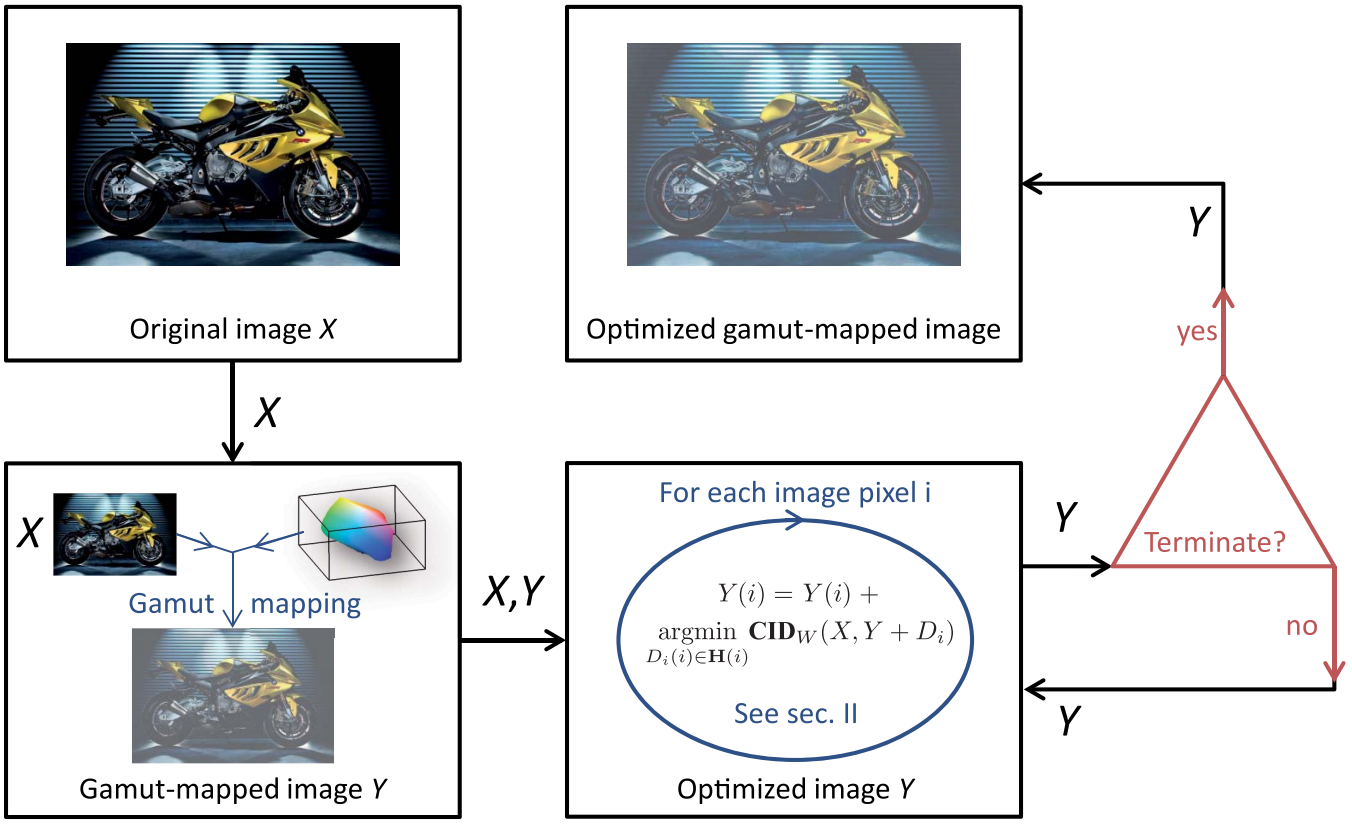

Fig. 1. Stages of the proposed iterative gamut-mapping optimization. Given the original image X and the gamut, a gamut-mapping algorithm yields an image Y. Then, the CID metric is minimized for each image pixel i according to Section II (global iteration). The global iterations are repeated for the optimized gamut-mapped image Y until the termination condition is fulfilled.

Let us assume that the image Y is within the gamut of the device, i.e., $Y \widetilde{\subset} \mathbf{G}$. Then, an image $Z \widetilde{\subset} \mathbf{G}$ satisfying $\mathbf{CID}_\Omega(X, Z) \leq \mathbf{CID}_\Omega(X, Y)$ can be obtained as follows:

$$Z(i) = Y(i) + \underset{D_i(i)\in\mathbf{H}(i)}{\operatorname{argmin}} \mathbf{CID}_W(X, Y + D_i), \quad (6)$$

$$Z(j) = Y(j), \quad j \neq i, \quad (7)$$

where all variables are defined as above, $i \in \Omega$ is an arbitrary pixel position, and

$$\mathbf{H}(i) = \left\{ d \in \{-\epsilon_{\mathrm{JND}}, 0, \epsilon_{\mathrm{JND}}\}^3 \mid Y(i) + d \in \mathbf{G} \right\}. \quad (8)$$

In other words: to minimize the global CID metric $\mathbf{CID}_\Omega$, we improve the image Y only at pixel position i by minimizing the local CID metric $\mathbf{CID}_W$. Note that the definition of $\mathbf{H}(i)$ ensures that the pixel's color stays in-gamut and that $\mathbf{CID}_W$ needs to be evaluated maximally 27 times to find the minimum. Due to the small number of evaluations, a brute-force computation is reasonable. The evaluations can be performed very efficiently since some comparison terms stay constant for multiple elements of $\mathbf{H}(i)$, e.g., the lightness-related comparison terms (l_L, c_L, s_L) must be computed only for three lightness levels considered in $\mathbf{H}(i)$. Furthermore, non-constant comparison terms corresponding to different elements of $\mathbf{H}(i)$ deviate only by computationally inexpensive terms. Therefore, a mathematically simple update of the corresponding comparison terms deduced from Equations (16)–(20) (see Appendix A) is possible for recomputation.

Algorithm 1 Optimizing Gamut Mapping

INPUT: gamut $\mathbf{G}$, reference image X

1. $Y = \mathcal{G}(X) \widetilde{\subset} \mathbf{G}$
2. **REPEAT**
3. **FOR EACH** $i \in \Omega$
4. $Y(i) = Y(i) + \operatorname{argmin}_{D_i(i)\in\mathbf{H}(i)} \mathbf{CID}_W(X, Y + D_i)$
5. **END FOR**
6. **UNTIL** TERMINATE

OUTPUT: Y

For solving the discrete version of problem (2), Equation (6) is applied iteratively for all image pixels $i \in \Omega$ yielding **Algorithm 1**. Note that a gamut-mapping transformation $\mathcal{G}$ must initially be applied to the input image X ensuring a valid in-gamut image for the iteration. Pixel-wise gamut-mapping transformations, e.g., as included in ICC profiles [24], may be used. Fig. 1 illustrates the optimization methodology.

We denote one execution of the inner-loop (lines 3-5 in **Algorithm 1**) as one *global iteration*. A global iteration can be executed in parallel as long as all concurrent pixel optimizations belong to mutually non-overlapping windows. Various termination conditions for the global iteration (see line 6 in **Algorithm 1**) may be used (e.g., if changes of CID between two global iterations fall below a predefined threshold). In the experiment, a fixed number (=30) of global iterations was used to terminate the optimization.

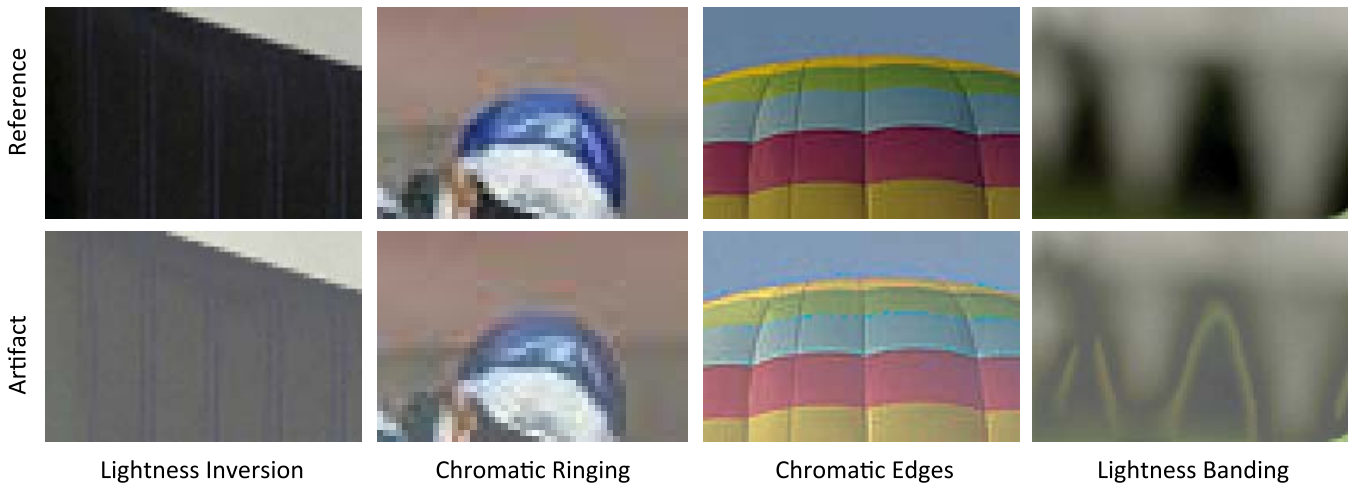

Fig. 2. Artifacts illustrating the shortcomings of the CID metric when used for optimizing gamut mapping.

The optimization was tested on five images, a very small gamut (extracted from the `USNewsprintSNAP2007.icc` profile) and two gamut-mapping algorithms for $\mathcal{G}$ (CLIPSLIN and SGCK [7]). A visual paired-comparison experiment with thirteen unbiased color-normal observers shows that more than 90% of all decisions rated the optimized images to be more similar to the original than the initial gamut-mapped images. More details on the experiment and the optimized images are given in [13]. Even though the predicted and the perceived image differences were both improved, almost all resulting images possessed clearly apparent artifacts, particularly: lightness inversion, chromatic ringing, chromatic edges, and lightness banding, as illustrated in Fig. 2. The artifacts are created after some iterations of the optimization algorithm and decrease the perceived image difference noticeably. This indicates that the property shown in Equation (1) is not satisfied for the CID metric and that there is some room for improving the metric by low-level (non-semantic) means.

Our paper addresses these shortcomings and extends previous work [9], [13] by the following key contributions:

1) We modify the CID metric to avoid optimization artifacts.
2) The resulting *improved CID* (iCID) metric is evaluated on gamut-mapping and conventional visual databases.
3) A visual experiment is presented that compares the iCID-based gamut-mapping optimization with a state-of-the-art gamut-mapping algorithm.
4) We introduce optimization intents to account for specific application purposes.

III. Improving the CID Metric

For improving the CID metric, we must analyze all artifacts created by the optimization. Adjustments and further modifications of the metric are required to avoid predictions inconsistent with our perception. In the following, we address each artifact and propose modifications of the CID metric to obtain artifact-free optimization results.

A. Lightness Inversion

Fig. 2 shows an example of this artifact: in the reference image the background is darker than the stripes whereas it is brighter in the gamut-mapped image below. The CID metric is able to detect lightness inversion by its lightness-difference comparison term (see Equation (16) in Appendix A). It can be shown that an image without lightness inversion has a smaller predicted difference to the reference than the same image possessing this artifact. Therefore, it is unlikely that this artifact is created by the optimization. However, if the input image $Y = \mathcal{G}(X)$ contains lightness-inversion artifacts, they are preserved or even amplified by the optimization. This is because lightness-contrast and lightness-structure are not affected by lightness inversion and the CID metric gives more weight to lightness-contrast and lightness-structure differences (see Equations (17), (18) in Appendix A) than to lightness differences (see Equation (16) in Appendix A). If the input image already includes lightness-inversion artifacts, the iteration runs into a local minimum preserving or nearly fully reconstructing lightness-contrast and lightness-structure. The artifact is therefore a local minimum of the objective function resulting from an inappropriate starting image. This was confirmed by analyzing the input images in the experiment. They already contained lightness-inversion artifacts which were introduced by the initial gamut mapping.

We can avoid lightness-inversion artifacts by employing an initial gamut mapping $\mathcal{G}$ that transforms lightness monotonically, i.e., for $Y = \mathcal{G}(X) : X_L(i) \leq X_L(j) \Rightarrow Y_L(i) \leq Y_L(j)$, where X_L, Y_L are the lightness components of the images X, Y and $i, j \in \Omega$ are arbitrary pixel positions. Note that gamut-mapping transformations incorporated in ICC profiles usually satisfy this conditions.

B. Chromatic Ringing

This artifact can be described by chromatic lines repeating the shape of an image edge. Fig. 2 shows an example. Chromatic ringing occurs only in the chroma channel. Hue is not affected. The CID metric accounts for chroma deviations

only with its chroma-difference term (see Equation (19) in Appendix A) which compares only weighted average chroma values. This is insufficient to detect chroma-contrast variations and leaves too many degrees-of-freedom in the chroma channel for the optimization. To avoid ringing artifacts, we add a chroma-contrast comparison term c_C to the CID metric. This term is defined analogously to the lightness-contrast comparison term (see Equation (17) in Appendix A) but uses chroma instead of lightness components:

$$c_C(\mathbf{x},\mathbf{y}) = \frac{2\sigma_{\mathbf{x}}^C\sigma_{\mathbf{y}}^C + c_6}{{\sigma_{\mathbf{x}}^C}^2 + {\sigma_{\mathbf{y}}^C}^2 + c_6}, \tag{9}$$

where $\mathbf{x},\mathbf{y}$ are the pixel arrays within the window, $\sigma_{\mathbf{x}}^C, \sigma_{\mathbf{y}}^C$ are the Gaussian-weighted standard deviations of the chroma components computed for the pixel arrays, and $c_6 > 0$ is a weighting parameter. For improving the CID metric, c_C is included as an additional factorial term into Equation (3). No ringing artifacts are created by the optimization if the resulting CID metric is used as the objective function.

C. Chromatic Edges

This artifact describes a contouring of image edges by a thin chromatic line as shown in Fig. 2. It affects only the chroma channel and is not penalized by the CID metric even when improved by the chroma-contrast comparison term (see Equation (9)). Chromatic edges bias the chroma structure of the original image. In order to account for this artifact, we add a chroma-structure comparison term s_C to the CID metric. It is similarly defined as the lightness-structure comparison term (see Equation (18) in Appendix A) but uses chroma instead of lightness:

$$s_C(x,y) = \frac{|\sigma_{\mathbf{xy}}^C| + c_7}{\sigma_{\mathbf{x}}^C\sigma_{\mathbf{y}}^C + c_7}, \tag{10}$$

where $\mathbf{x}$ and $\mathbf{y}$ are the pixel arrays within the window, $\sigma_{\mathbf{xy}}^C$ is the Gaussian-weighted linear correlation of chroma components between the pixel arrays, $\sigma_{\mathbf{x}}^C$ and $\sigma_{\mathbf{y}}^C$ are defined as in Equation (9), and $c_7 > 0$ is a weighting parameter. Optimized images are free from chromatic-edge artifacts if the CID metric contains the chroma-structure comparison term.

D. Lightness Banding

We refer to banding artifacts as mostly elongated structures – absent in the reference image – which appear in the lightness channel of the optimized image. An example is shown in Fig. 2. The lightness-structure comparison term (see Equation (18) in Appendix A) detects banding, but its influence within the CID metric is obviously too small for inhibiting this artifact. The contribution of the lightness-structure comparison term cannot be sufficiently increased by adjusting the weighting parameter c_3. Therefore, we introduce an exponential parameter $\alpha > 1$ to increase the relative importance of the lightness-structure comparison term as $s_L(\mathbf{x},\mathbf{y})^\alpha$. Exponential parameters were already proposed for the SSIM index to weight the contribution of involved terms [8].

The larger α, the more important is the lightness-structure comparison term within the CID metric. Banding artifacts were completely inhibited by an appropriate magnitude of α determined by the parameter study described below.

E. Improved CID Metric

Combining all modifications results in the **i**mproved **C**olor-**I**mage **D**ifference (**iCID**) metric:

$$\begin{aligned}\mathbf{iCID}_A(X,Y) &= 1 - \frac{1}{|A|}\sum_{i\in A}\Big[l_L(\mathbf{x}_i,\mathbf{y}_i)\cdot c_L(\mathbf{x}_i,\mathbf{y}_i)\cdot s_L(\mathbf{x}_i,\mathbf{y}_i)^\alpha \cdot l_C(\mathbf{x}_i,\mathbf{y}_i) \\ &\qquad \cdot l_H(\mathbf{x}_i,\mathbf{y}_i)\cdot c_C(\mathbf{x}_i,\mathbf{y}_i)\cdot s_C(\mathbf{x}_i,\mathbf{y}_i)\Big]\end{aligned} \tag{11}$$

where l_L, c_L, s_L, l_C, and l_H are defined equally as in the CID metric (see Equations (16)–(20) in Appendix A), c_C is the new chroma-contrast comparison term defined in (9) and s_C is the new chroma-structure comparison term defined in (10). Other variables are defined analogously as in (3). We want to emphasize that the RGB input images X and Y are initially normalized to reference viewing conditions by an image-appearance model and then transformed into the LAB2000HL color space [23]. As explained in Appendix A, this is performed by the transformation $\mathbf{N}$ (see [9] for more details). The pixels in the window arrays $\mathbf{x}_i$, $\mathbf{y}_i$ are extracted from the resulting LAB2000HL images X_{norm} and Y_{norm}. In Equation (11) this initial transformation is not shown for the sake of readability.

F. Adjusting the Parameters

The iCID metric has a total of ten parameters (not counting parameters to specify the viewing conditions): the weighting parameters $c_1,\ldots,c_7$, α, the window size k, and the standard deviations σ_G for computing the Gaussian weights used by the comparison terms (see Appendix A). For reasons given in the introduction, fitting the parameters to visual databases containing gamut-mapping distortions is highly biased by heuristics employed by the gamut-mapping algorithms. Unfortunately, adjusting iCID parameters by optimizing gamut mapping as described in Section II-B is a "chicken-and-egg problem": to judge which parameter set yields better optimization results (in terms of perceived deviations from the original image), a perception-based IDM is required. Due to the large number of parameters, replacing the metric by visual judgments is impractical as well.

However, there are good reasons to assume that multiple parameters can be set equally without adversely affecting iCID's prediction performance: the weighting parameters $c_1,\ldots,c_7$ highly depend on the properties of the working color space. Since all image comparison terms operate on the nearly perceptually uniform LAB2000HL color space, c_i parameters belonging to terms with a similar structure can be assumed to have the same magnitude. Particularly, parameters c_1, c_4, and c_5 contained in the lightness-difference, chroma-difference, and hue-difference term can be assumed to be similar, i.e., $c_1 = c_4 = c_5$. Note that the LAB2000HL color

space was designed for perceptual uniformity, meaning that equal Euclidean distances have nearly the same perceived color difference independently in what attribute – lightness, chroma, and hue – the colors differ the most.

If the image-appearance-model transformation **N** considers the difference of the human visual system's chromatic and achromatic contrast sensitivities by appropriately blurring the input images (see [25]), parameters c_2 and c_6 within the lightness-contrast and chroma-contrast comparison terms can be assumed to be similar as well, i.e., $c_2 = c_6$. This is because both contrast comparison terms operate on LAB2000HL images whose achromatic and chromatic spatial-frequency components are normalized by **N**. In combination with the perceptual uniformity of LAB2000HL, predicted lightness-contrast and chroma-contrast deviations of equal magnitude are (ideally) perceived equally. Since this also applies to the lightness-structure and chroma-structure comparison term, we set $c_3 = c_7$. To further reduce the number of effective parameters, we assume that the lightness-contrast and lightness-structure parameters, c_2 and c_3, are equal and thus $c_2 = c_3 = c_6 = c_7$. Note that the relative importance of the lightness-structure term can be additionally adjusted by α. In summary, we reduce the seven c_i parameters to only two effective parameters by setting $c_1 = c_4 = c_5$ and $c_2 = c_3 = c_6 = c_7$.

We keep the window size $k = 11$ as in the CID metric but slightly increase the standard deviation σ_G (see Appendix A) from $\sigma_G = 1.5$ to $\sigma_G = 2$. This gives more weight to edge pixels of the window and reduces lightness-banding artifacts within images resulting from the gamut-mapping optimization. Please note that k and σ_G are suitable for typical display viewing conditions of roughly 40 pixels per degree of visual field [8], [9]. This applies, for instance, to a display with a screen width of 50 cm covered by 1600 pixels at a viewing distance of 70 cm. If the viewing conditions severely deviate from this value, the input images should be rescaled appropriately. Otherwise, the window size k would not correspond to the image scale the iCID metric is working on.

We used a two-stage strategy for adjusting the remaining three effective parameters ($c_1 = c_4 = c_5$, $c_2 = c_3 = c_6 = c_7$, and α). In the first stage, we set $\alpha = 1$. The remaining two parameters were varied as follows: $c_1 = c_4 = c_5 = 0.0002, 0.002, 0.02, 0.2$ and $c_2 = c_3 = c_6 = c_7 = 0.01, 0.1, 1, 10$. For each parameter combination, iCID-based gamut-mapping optimizations were computed as described in Section II-B for 14 reference images (examples are shown in Figs. 4 and 5). The gamut as well as the initial gamut mapping (ICC perceptual intent [24]) were extracted from the `USNewsprintSNAP2007.icc` profile. Results were visually inspected only with respect to artifacts by three color-normal expert observers. The parameter combination showing the best result regarding lightness-banding artifacts was chosen for the next stage. The other parameter combinations yield more artifacts or artifacts which are more disturbing.

Parameter variations were performed logarithmically in the first stage because iCID-based gamut-mapping optimizations are very insensitive to small changes of c_i parameters. This agrees with observations made for the prediction performance of the CID metric [9].

TABLE I
PARAMETERS OF THE iCID METRIC

c_1, c_4, c_5	c_2, c_3, c_6, c_7	α	k	σ_G
0.002	10	3	11	2.0

In the second stage, the parameter α was increased ($\alpha = 1, 2, \ldots$), keeping the other parameters constant. For each α, iCID-based gamut-mapping optimizations were computed for the same images and settings as in stage one. The smallest α was selected so as to yield artifact-free results. Table I shows the best set of parameters which we use in the following.

We want to emphasize that the described parameter adjustment might not be optimal with respect to iCID's prediction performance. However, it yields artifact-free iCID-based gamut-mapping optimizations. Note that only three weighting parameters are employed by the iCID metric which speaks for a high generalization ability with respect to artifact-free optimizations. We validated this on various other reference images and gamuts.

IV. Results and Discussion

Our approach for developing the iCID metric deviates fundamentally from conventional approaches. Instead of maximizing iCID's prediction performance on visual datasets, we aimed to enhance its properties as an objective function for optimizing gamut mapping particularly with respect to avoiding artifacts. Even though there are good reasons (described in the introduction) not to rely on visual datasets for developing an IDM, the agreement between predictions and subjective scores remains the key figure-of-merit to judge a metric's performance.

Therefore, we investigate iCID's prediction performance on visual datasets comprising gamut mapping and conventional distortions. We are particularly interested if the modifications have any adverse effect in this regard.

Furthermore, we compare iCID-based gamut-mapping optimizations with results of a state-of-the-art spatial gamut-mapping algorithm. Finally, we show how different gamut-mapping optimization intents might be achieved by tuning iCID's parameters.

A. Image-Appearance Model

In this paper, all visual datasets used to evaluate the prediction performance were created by display-based experiments in indoor environments. Even though the exact viewing-condition parameters (e.g., luminance level) are not available, they can be assumed to be close to the reference viewing conditions of the LAB2000HL color space. Therefore, we considered only the visual resolution for normalizing the input images by the initial transformation **N** (see Equation (13) in Appendix A). For this, images were filtered by achromatic and chromatic contrast-sensitivity functions (CSFs) assuming 40 pixels per degree. We adopted the CSFs proposed for predicting image differences by the iCAM framework [26]. These CSFs are applied in the frequency domain on images transformed into

TABLE II
HIT RATES ON THE GAMUT-MAPPING DATABASE

	CID	iCID*	iCID
None	0.674	0.677	0.668
CSF	0.676	0.676	0.673
SSIM	0.665		
FSIMc	0.641		
MSSIM	0.638		
FSIM	0.637		
UQI	0.630		
VIF	0.597		
NQM	0.590		
VSNR	0.587		
VIFP	0.582		
SNR	0.572		
PSNR	0.572		
MSE	0.572		
WSNR	0.564		
IFC	0.558		

* without chroma-contrast and -structure term

the intensity-linear YCC opponent color space. Space and CSFs are designed for filtering the achromatic channel without perceptible influence on the chromatic channels and vice versa. We followed the recommendation from Johnson and Fairchild [27] and turned the bandpass-shaped achromatic CSF into a lowpass to avoid filtering artifacts. To investigate the importance of normalizing the images with respect to the visual resolution, we present all results with CSF filtering (denoted as **CSF**) and without filtering (denoted as **None**).

B. iCID's Performance on Gamut-Mapping Distortions

We evaluated iCID's prediction performance on a large visual database of gamut-mapping distortions. This database was already used for studying the CID metric [9]. It is a combination of six gamut-mapping datasets [18], [22], [28]–[30] from different paired-comparison experiments including 326 reference images, 2,659 distorted images, and 29,665 decisions made by subjects.

As a performance indicator, we used the hit rate which is the fraction of paired-comparison decisions correctly predicted by the metric, i.e., hit rate $= T/A$, where T is the number of correctly predicted decisions and A is the number of all decisions excluding ties. Note that due to contradicting decisions of the subjects for the same comparison the best achievable hit rate called *majority hit rate* is $\hat{p}_m = 0.806$. Lissner et al. [9] introduced a test to check whether the hit rates of two metrics are significantly different or only the result of chance. It is based on Yule's two-sample binomial test [31]. For our combined visual database of gamut-mapping distortions, a hit-rate difference of 0.008 and higher is significant.

Table II shows the hit rates. Note that they differ from the results given by Lissner et al. [9] who used a fraction of this database for parameter fitting and only the remaining data for performance testing, i.e., for computing hit rates.

According to Yule's two-sample binomial test [31], the CID metric and the iCID metric do not perform significantly differently if CSF filtering is considered (second row in Table II). This is quite interesting and the main result of this investigation because the CID metric was partly fitted to the database and iCID's parameters are adjusted independently.

The chroma-contrast and chroma-structure terms have a significantly negative impact on the prediction performance if CSF filtering is not performed (see the first row in Table II). CSF filtering seems to be crucial for maximizing iCID's prediction performance for typical gamut-mapping distortions because it reduces the impact of the chroma-contrast and chroma-structure term compared to the corresponding lightness terms.

Table II shows also results for the MeTriX MuX Package [10] as well as for the FSIM and FSIMc index [32]. The MeTriX MuX Package includes SSIM [8], MSSIM [11], UQI [33], VIF and VIFP [12], NQM [34], VSRN [35], WSNR [36], IFC [37], signal-to-noise ratio (SNR), peak signal-to-noise ratio (PSNR), and mean squared error (MSE). The best performing IDM amongst these is the SSIM index with a hit rate of 0.665. Even though SSIM performs significantly worse compared to both the CID metric and the iCID metric, its hit rate is astonishingly large on the whole gamut-mapping database considering that it completely disregards chromatic information. A plausible explanation is related to the design of the gamut-mapping database and particularly to the algorithms used to create the distortions. All algorithms almost preserve hue. The impact of chroma variations on subjective scores was highly limited by the fact that images presented in each paired comparison were mapped to the same gamut. Hence, subjective decisions collected in this database were highly reduced to perceived differences in lightness-contrast and lightness-structure features, which are well predicted by SSIM. Chromatic information plays a significant but not a dominate role for predicting the impact of common gamut-mapping distortions on perceived image differences.

It is noteworthy that unlike conventional distortions (such as noise, blur, or compression artifacts), image-difference features highly correlate across scales for gamut-mapping distortions [9]. Therefore, employing multi-scale information as in the MSSIM [11] index does not improve the prediction performance on the gamut-mapping database.

C. iCID's Performance on Conventional Distortions

According to Lissner et al. [9], chromatic information is not essential for judging conventional distortions such as noise, blur, or compression artifacts. In this paper, we are interested in whether chroma-contrast and chroma-structure information considered by iCID impair the prediction performance compared to the CID metric. To investigate this aspect, we used the Tampere Image Database 2013 (TID2013) [38] comprising 3,000 conventionally distorted images originated from 25 reference images. More than 500,000 paired comparisons were evaluated by nearly 1,000 subjects.

The TID2013 provides only *Mean Opinion Scores* (MOS) and no individual paired-comparison choices. Therefore, the Spearman rank-order correlation [5] was used as a

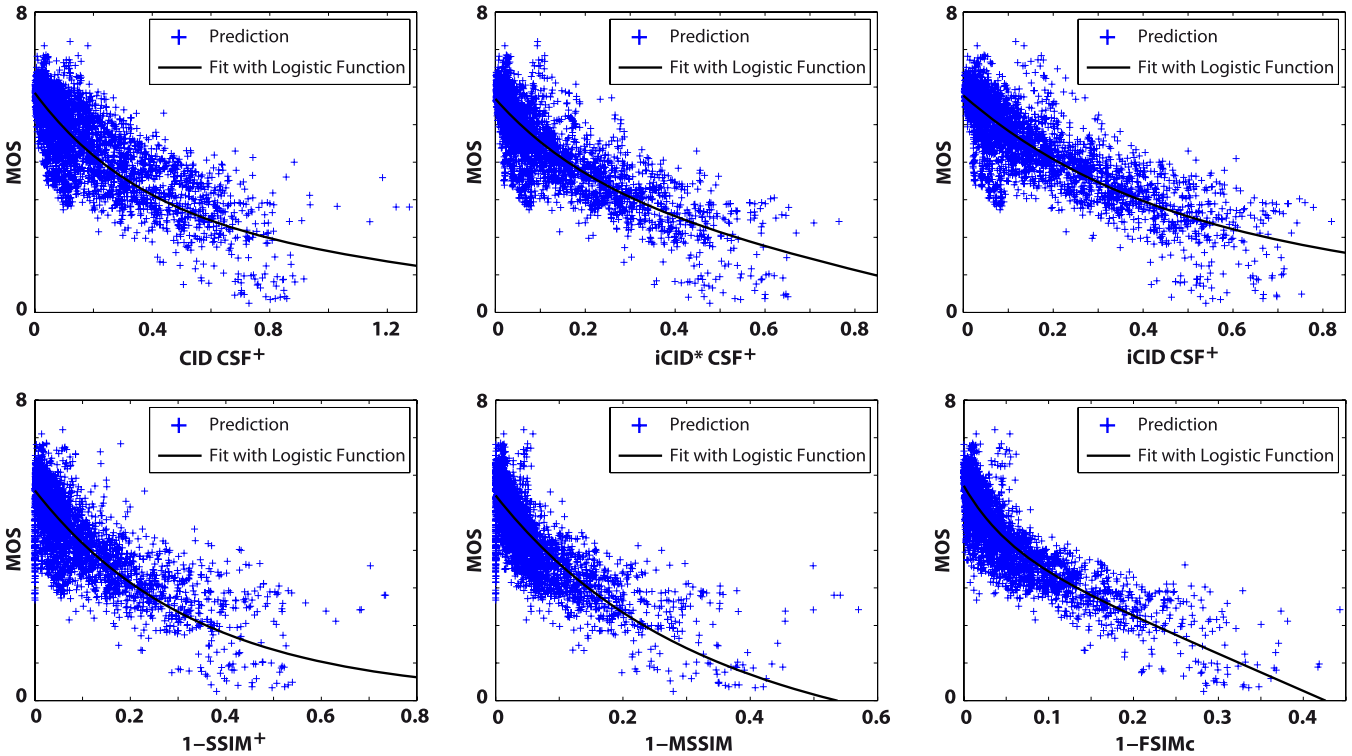

Fig. 3. Scatter plots of subjective scores (MOS) against predictions of some image-difference metrics on the TID2013.

TABLE III
SPEARMAN CORRELATIONS ON TID2013

	CID	iCID*	iCID
None	0.604	0.656	0.501
None$^+$	0.752	0.813	0.705
CSF	0.666	0.713	0.693
CSF$^+$	0.773	0.823	0.813
SSIM	0.627		
SSIM$^+$	0.742		
MSSIM	0.785		
FSIMc	0.851		
FSIM	0.802		

* without chroma-contrast and -structure term
$^+$ automatic downsampling

performance indicator. An absolute correlation value of 1 means a perfect match to subjective scores whereas a value of 0 means no correlation at all.

Image-difference features are much less correlated across scales for conventional distortions than for gamut-mapping distortions. Therefore, we considered an automatic downsampling to compute the CID metric and the iCID metric on a scale for which the human visual system is particularly sensitive. This automatic downsampling was introduced in a recent implementation of the SSIM index [8], [39] and was adapted for the CID metric and the iCID metric for comparison. On the gamut-mapping database automatic downsampling has no significant effect on the hit rates of the CID metric and the iCID metric.

The results are summarized in Table III. They show that adding the chroma-contrast and chroma-structure terms clearly has a negative effect on the prediction performance if CSF filtering is not performed (see first two rows in Table III). The importance of these features is obviously overrated. CSF filtering highly blurs the chromatic components and lowers the influence of the chroma-contrast and chroma-structure terms within iCID. This improves its prediction performance considerably (see third and forth row in Table III). Since iCID's accuracy is still slightly lower when the terms are included, chromatic blurring caused by the applied CSF filters seems not to be sufficient. Results for the iCID metric might be improved by assuming a slightly higher pixels-per-degree value for filtering. The TID2013 does not provide any information in this regard.

Computing single-scale IDMs on the appropriate scale by automatic downsampling highly improves their prediction performance. A prerequisite for achieving high prediction rates with iCID for conventional distortions is a suitable chromatic and achromatic normalization of the input images with respect to visual resolution. This was less critical for the CID metric.

The downsampled iCID metric with CSF filtering shows a clearly better performance on the TID2013 than CID, SSIM, and MSSIM. The highest correlation is achieved by the FSIMc index [32] which, however, has a significantly worse hit rate on the gamut-mapping database (see Table II).

A more detailed investigation of the metrics' behavior on the TID2013 is given in Fig. 3. Scatter plots of MOS versus predictions are shown for some metrics of interest. The narrower the point cloud the better is the metric's performance. A group of outliers for the CID and iCID plots is in the region of MOS <4 and (i)CID <0.1. These points belong to the images with *local block-wise distortions of different intensity*

Fig. 4. Examples of iCID-based gamut-mapping optimizations compared to the ICC-based starting images. Reference images were taken from Wikimedia Commons [40], [41]. Best viewing conditions are on a display calibrated to sRGB.

indicating that (i)CID is not able to predict the perception of such distortions properly. SSIM$^+$ and MSSIM seem to fail to predict the distortion *change of color saturation* indicated by the line of points which is very close to the y-axis. This is quite reasonable as both metrics operate only on grayscale values in contrast to CID, iCID, and FSIMc.

D. Results for iCID-Based Gamut-Mapping Optimization

iCID's main advantage comes into play if used as an objective function for optimizing gamut mapping. iCID-based gamut-mapping optimizations are free from lightness-inversion, lightness-banding, chromatic-ringing, and chromatic-edge artifacts and retain contrast, structure, and color of the original images to a great extent.

We illustrate this in Fig. 4 using a very small gamut specified by the `USNewsprintSNAP2007.icc` profile. Its volume is less than 30% of the sRGB gamut if computed in the uniform LAB2000HL color space. In Fig. 4, reference images are shown on the left and iCID-based gamut-mapping optimizations on the right. The starting images of the optimizations are shown in the middle and were created by the pixel-wise gamut-mapping transformation incorporated in the ICC profile (perceptual intent). Note that the gray haze contained in the ICC-based images is almost removed by the optimization. Furthermore, chroma is restored to a great extent (e.g., the color of the sky and some colors in the balloons). In contrast to hue-preserving heuristics employed by common gamut-mapping algorithms, small hue shifts are introduced by the optimization for the benefit of gaining chroma.

We compare iCID-based optimization with a state-of-the-art spatial gamut-mapping algorithm proposed by Zolliker and Simon, called *Local Contrast Recovery* (LCR) [18]. LCR avoids artifacts by an unsharp masking technique based on edge-preserving smoothing. The LCR method requires also an initial gamut-mapping transformation. This transformation and the gamut were again extracted from the ICC-profile used before. Fig. 5 shows two reference images and the results of both approaches.

We can see that structure and contrast are well retained by both approaches. Compared to the pixel-wise ICC-based gamut mapping (not shown in the Figure), haze is drastically reduced. The main difference between the resulting images is color. In this regard, LCR relies on the initial gamut-mapping transformation and is highly limited in exploiting the whole gamut. This is particularly apparent in the floor of the motorcycle image and in the sand and cloth of the desert image. In contrast, iCID-based optimizations are able to retain chroma to a great extent.

We conducted a paired-comparison experiment on 14 natural images mapped to the small gamut used above. Three gamut-mapping methods were compared: the ICC-based transformation with perceptual intent (denoted as ICC), the LCR method (denoted as LCR), and the iCID-based optimization (denoted as iCID optimized). We used the ICC-based gamut mapping as the initial transformation for the latter two. 15 color-normal unbiased observers participated in the experiment. A reference and two distorted images derived from the reference were shown simultaneously on a calibrated LCD-display. Observers were asked to select the distorted image which is more similar to the reference. Each observer made 42 decisions. Tie decisions were allowed and counted half the vote for each option. Results are collected in a frequency matrix, each element of which represents the number of decisions one method was preferred over another. iCID-based optimizations were selected in 95% of all

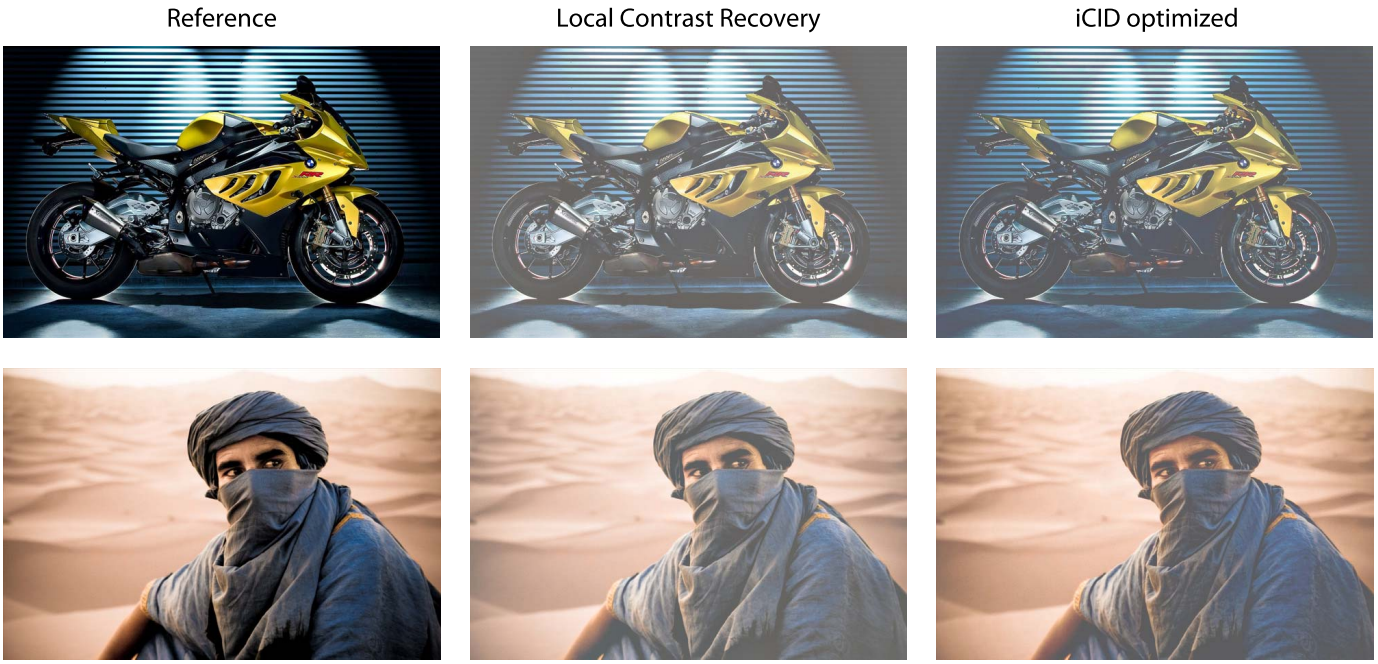

Fig. 5. Examples of iCID-based gamut-mapping optimization compared to Local Contrast Recovery. Reference images were taken from Wikimedia Commons [42] and from Fotopedia [43]. Best viewing conditions are on a display calibrated to sRGB.

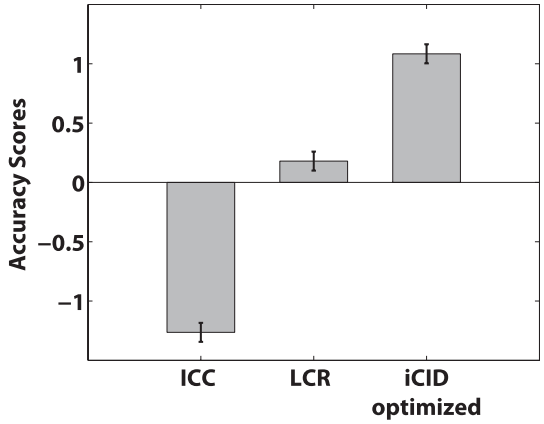

Fig. 6. Bar plot of the accuracy scores from the paired-comparison experiment. The error bars represent the 95% confidence interval.

decisions when compared with ICC-based gamut-mapped images and in 72% when compared with LCR results. Accuracy scores (averaged z-scores) were computed from the frequency matrix as described in [44]. Fig. 6 shows the results indicating that iCID-based optimizations were selected significantly more often than results of both other methods.

The results of the gamut-mapping optimization were also validated on a different, slightly larger gamut extracted from the FOGRA27 ICC-profile [45].

E. Optimization Intents

iCID-based gamut-mapping optimizations may yield hue shifts for the benefit of gaining chroma or contrast. This minimizes the predicted image difference to the original image, based on the low-level image-difference features employed by iCID. Unfortunately, it may adversely affect semantic information such as memory colors of objects (e.g., skin or brand colors). If, for instance, skin turns greenish, perceived image difference might increase drastically, even though structure and chroma are improved.

TABLE IV
OPTIMIZATION INTENTS FOR ICID-BASED GAMUT-MAPPING OPTIMIZATION

Optimization intent	c_4	c_5
perceptual	0.002	0.002
hue-preserving	0.002	0.02
chromatic	0.02	0.02

By varying iCID's chroma-difference and hue-difference parameters, c_4 and c_5, we are able to control the amount of chroma and hue shifts introduced by the optimization. Larger c_4 and c_5 parameters increase the importance of the corresponding terms preserving respective color attributes. We propose three parameter sets shown in Table IV (all other parameters remain unchanged) each defining one optimization intent for the iCID-based gamut-mapping optimization (Section II-B):

- **Perceptual:** allowing similar changes in lightness, chroma, and hue. Within the perceptually uniform LAB2000HL color space this is achieved by the default parameter set given in Table I.
- **Hue-preserving:** forces smaller deviations in hue.
- **Chromatic:** forces smaller deviations in chroma and hue. Optimization results are more chromatic without noticeable hue shifts at the expense of larger lightness variations.

Fig. 7 illustrates the impact of the optimization intents on the optimization results. Note that semantic maps of the image,

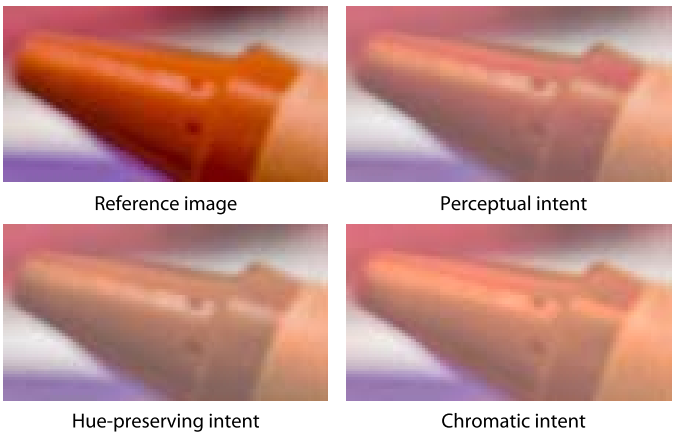

Fig. 7. Example of different optimization intents: the orange crayon's tip changes in chroma and hue. The image was taken from Fotopedia [46]. Best viewing conditions are on a display calibrated to sRGB.

e.g., resulting from skin or face detection algorithms, might be used to create spatially varying parameter sets preserving hues for memory colors and allowing hue shifts elsewhere.

V. Conclusion

The recently proposed *Color-Image-Difference* (CID) metric shows high prediction performance on visual datasets comprising gamut-mapping distortions. This made CID interesting to be used as an objective function for finding an in-gamut image with the smallest distance to the original. We presented a discrete iterative algorithm for optimizing gamut mapping with respect to CID, employing a fraction of the just-noticeable color difference as a local step length. An existing gamut-mapping algorithm is used to create an in-gamut starting image for the iteration.

Optimized images show a higher agreement with the original than the starting images, but were contaminated by various types of artifacts. We addressed these artifacts by multiple modifications yielding the *improved Color-Image-Difference* (iCID) metric. The prediction performance on visual data comprising gamut-mapping and conventional distortions was improved by the modifications. Note that iCID's prediction scores are more sensitive to an appropriate chromatic and achromatic normalization of the input images with respect to the visual resolution.

The proposed modifications allow artifact-free gamut-mapping optimizations retaining contrast, structure, and particularly color of the original image to a great extend. To our knowledge iCID is the only image-difference metric with these capabilities. A visual experiment revealed that – with respect to the perceived difference between original and gamut-mapped images – iCID-based gamut-mapping optimization significantly outperformed a state-of-the-art spatial gamut-mapping algorithm.

We believe that iCID combined with the gamut-mapping optimization may help to gain new insights of the importance of single (low-level) image-difference attributes in the scope of color-image reproduction. Linking iCID with semantic information of the image (obtained, e.g., by face-recognition algorithms) may allow spatially-varying iCID parameters for adjusting the importance of distinct low-level difference-attributes to the image content (e.g., by increasing the importance of hue for memory colors). Future research shall address this approach to further improve the prediction performance on visual data and gamut-mapping optimizations.

We provide a MATLAB implementation of iCID and executables of the gamut-mapping-optimization algorithm on our website [47].

Appendix
The Color-Image-Difference Metric

The Color-Image-Difference (CID) metric is a particular implementation of the color-image-difference framework proposed by Lissner et al. [9]. A sketch of this framework is shown in Fig. 8. The input of the metric are two RGB images X, Y and information of particular viewing conditions (viewing distance, adapting luminance, etc.). In the first processing step, the images are normalized to reference viewing conditions by an image-appearance model and transformed into a working color space. Image-appearance models tested in [9] consider only the viewing distance by contrast-sensitivity filtering. For the working color space, the nearly perceptually uniform and hue linear LAB2000HL color space [23] was chosen as suggested in [9]. From the resulting two LAB2000HL images so-called Image-Difference Features (IDFs) are extracted. IDFs are mathematical formulations of hypothesis on the image-difference perception. Finally, all IDFs are combined into a single value representing the prediction of the perceived image difference under the particular viewing conditions.

The following mathematical description of the CID metric is partly extracted from [9]. Each IDF can be written as the concatenation of a normalizing transformation $\mathbf{N}$ and a transformation describing the feature extraction $\mathbf{F}$.

$$\mathbf{IDF} = \mathbf{F} \circ \mathbf{N}, \tag{12}$$

where

$$\mathbf{N}: \ \mathcal{I}_{M,N} \times \mathcal{I}_{M,N} \times \mathcal{P} \rightarrow \mathcal{W}_{M,N} \times \mathcal{W}_{M,N}, \tag{13}$$

$$\mathbf{F}: \ \mathcal{W}_{M,N} \times \mathcal{W}_{M,N} \rightarrow [0, 1], \tag{14}$$

and $\mathcal{I}_{M,N}$ is the set of colorimetrically specified RGB images and $\mathcal{W}_{M,N}$ is the set of images in the working color space with M rows and N columns. $\mathcal{P}$ is a set of parameter arrays, each of which parametrizes the employed image-appearance model. Please note that various image-appearance models considering different viewing-condition attributes may be used for $\mathbf{N}$. All IDFs used by the CID metric must share the same normalizing transformation $\mathbf{N}$. Since the focus of the present paper lies on the feature-extraction transformations, $\mathbf{N}$ is not further specified here.

Each feature-extraction transformation $\mathbf{F}$ is the average over local image differences specified by an image-comparison transformation $\mathbf{t}$:

$$\mathbf{F}(X_{\text{norm}}, Y_{\text{norm}}) = \frac{1}{\mathrm{K}} \sum_{i=1}^{K} \mathbf{t}(\mathbf{x}_i, \mathbf{y}_i), \tag{15}$$

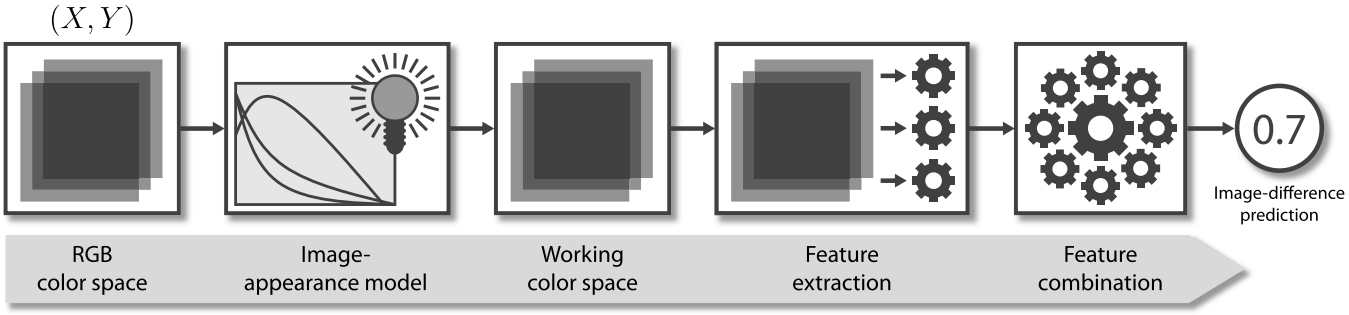

Fig. 8. CID framework as introduced by Lissner et al. [9].

where K is the number of considered image subregions within the normalized images $X_{\text{norm}}, Y_{\text{norm}} \in \mathcal{W}_{M,N}$ and $\mathbf{x}_i, \mathbf{y}_i$ are the corresponding pixel arrays defined by the i-th image subregion. In this paper, image subregions are sliding $k \times k$ windows ($k = 11$ by default). For the CID metric, five IDFs are defined covering lightness-difference $\mathbf{L}_L$, lightness-contrast $\mathbf{C}_L$, lightness-structure $\mathbf{S}_L$, chroma-difference $\mathbf{L}_C$, and hue-difference $\mathbf{L}_H$. The corresponding image-comparison transformations $\mathbf{t}$, denoted by l_L, c_L, s_L, l_C, and l_H, are adapted from the SSIM index [8] but are adjusted to the nearly perceptually uniform LAB2000HL color space:

$$l_L(\mathbf{x}, \mathbf{y}) = \frac{1}{c_1 \cdot \overline{\Delta L(\mathbf{x}, \mathbf{y})}^2 + 1}, \tag{16}$$

$$c_L(\mathbf{x}, \mathbf{y}) = \frac{2\sigma_{\mathbf{x}}\sigma_{\mathbf{y}} + c_2}{\sigma_{\mathbf{x}}^2 + \sigma_{\mathbf{y}}^2 + c_2}, \tag{17}$$

$$s_L(\mathbf{x}, \mathbf{y}) = \frac{|\sigma_{\mathbf{xy}}| + c_3}{\sigma_{\mathbf{x}}\sigma_{\mathbf{y}} + c_3}, \tag{18}$$

$$l_C(\mathbf{x}, \mathbf{y}) = \frac{1}{c_4 \cdot \overline{\Delta C(\mathbf{x}, \mathbf{y})}^2 + 1}, \tag{19}$$

$$l_H(\mathbf{x}, \mathbf{y}) = \frac{1}{c_5 \cdot \overline{\Delta H(\mathbf{x}, \mathbf{y})}^2 + 1}, \tag{20}$$

where $\mathbf{x}, \mathbf{y}$ are the pixel arrays within the window, $\sigma_{\mathbf{x}}, \sigma_{\mathbf{y}}$ are the Gaussian-weighted standard deviations of the lightness components, $\sigma_{\mathbf{xy}}$ describes the Gaussian-weighted linear correlation of both windows in the lightness channel, and $\overline{f(\mathbf{x}, \mathbf{y})}$ denotes the Gaussian-weighted mean of $f(x, y)$ computed for each pixel pair (x, y) in the window. The Gaussian weight distributions are all specified by the standard deviation σ_G. The pixel-wise transformations used above are defined as:

$$\Delta L(x, y) = L_x - L_y, \tag{21}$$

$$\Delta C(x, y) = C_x - C_y, \tag{22}$$

$$\Delta H(x, y) = \sqrt{(a_x - a_y)^2 + (b_x - b_y)^2 - \Delta C(x, y)^2}, \tag{23}$$

where a pixel $x = (L_x, a_x, b_x)$ has a lightness (L_x) and two chromatic components (a_x, b_x) and $C_x = \sqrt{a_x^2 + b_x^2}$ defines its chroma (analog definition for y). Table V shows the parameters of the CID metric as proposed in [9].

The CID prediction as described by Lissner et al. [9] is the following combination of IDFs (arguments are omitted for the sake of brevity):

$$\mathbf{CID} = 1 - \mathbf{L}_L\mathbf{C}_L\mathbf{S}_L\mathbf{L}_C\mathbf{L}_H. \tag{24}$$

For optimizing gamut mapping, a minor modification of the CID metric is required as described by Preiss and Urban [13]. Instead of computing all IDFs separately and combining them according to Equation (24), the image-comparison terms are multiplied pixel-wise and then averaged (see Equation (3)). This does not significantly change the performance on all visual databases considered in [9]. The CID metric improved in this paper refers to the definition by Preiss and Urban [13].

TABLE V
PARAMETERS OF THE COLOR-IMAGE-DIFFERENCE (CID) METRIC

c_1	c_2	c_3	c_4	c_5	k	σ_G
0.002	0.1	0.1	0.002	0.008	11	1.5

ACKNOWLEDGMENT

The authors thank Peter Zolliker for applying the Local Contrast Recovery algorithm on test images, Jana Blahová for conducting the visual experiment, and the Deutsche Forschungsgemeinschaft (German Research Foundation).

REFERENCES

[1] R. Eskew, Jr., "Higher order color mechanisms: A critical review," *Vis. Res.*, vol. 49, no. 22, pp. 2686–2704, 2009.
[2] D. Chandler, "Seven challenges in image quality assessment: Past, present, and future research," *ISRN Signal Process.*, vol. 2013, pp. 905685-1–905685-53, Feb. 2013.
[3] H. R. Sheikh, M. F. Sabir, and A. C. Bovik, "A statistical evaluation of recent full reference image quality assessment algorithms," *IEEE Trans. Image Process.*, vol. 15, no. 11, pp. 3441–3452, Nov. 2006.
[4] N. Bonnier, F. Schmitt, and H. Brettel, "Evaluation of spatial gamut mapping algorithms," in *Proc. 14th Color Imag. Conf. IS&T/SID*, Scottsdale, AZ, USA, 2006, pp. 56–61.
[5] C. Spearman, "The proof and measurement of association between two things," *Amer. J. Psychol.*, vol. 15, no. 1, pp. 72–101, Jan. 1904.
[6] M. G. Kendall, "A new measure of rank correlation," *Biometrika*, vol. 30, nos. 1–2, pp. 81–89, 1938.
[7] J. Morovič, *Color Gamut Mapping*. New York, NY, USA: Wiley, 2008.
[8] Z. Wang, A. C. Bovik, H. R. Sheikh, and E. P. Simoncelli, "Image quality assessment: From error visibility to structural similarity," *IEEE Trans. Image Process.*, vol. 13, no. 4, pp. 600–612, Apr. 2004.
[9] I. Lissner, J. Preiss, P. Urban, M. S. Lichtenauer, and P. Zolliker, "Image-difference prediction: From grayscale to color," *IEEE Trans. Image Process.*, vol. 22, no. 2, pp. 435–446, Feb. 2013.
[10] (2011, Apr. 15). *MeTriX MuX Version 1.1 Visual Quality Assessment Package* [Online]. Available: http://foulard.ece.cornell.edu/gaubatz/metrix_mux/

[11] Z. Wang, E. P. Simoncelli, and A. C. Bovik, "Multi-scale structural similarity for image quality assessment," in *Proc. IEEE 37th Asilomar Conf. Signals, Syst. Comput.*, vol. 2. Nov. 2003, pp. 1398–1402.
[12] H. Sheikh and A. Bovik, "Image information and visual quality," *IEEE Trans. Image Process.*, vol. 15, no. 2, pp. 430–444, Feb. 2006.
[13] J. Preiss and P. Urban, "Image-difference measure optimized gamut mapping," in *Proc. 20th Color Imag. Conf. IS&T/SID*, Los Angeles, CA, USA, 2012, pp. 230–235.
[14] L. A. Taplin and G. M. Johnson, "When good hues go bad," in *Proc. Conf. Color Graph., Imag., Vis.*, 2004, pp. 348–352.
[15] J. J. McCann, "Color gamut mapping using spatial comparisons," *Proc. SPIE, Color Imag., Device-Independ. Color, Color Hardcopy, Graph. Arts VI*, vol. 4300, pp. 126–130, Jan. 2001.
[16] J. Morovic and Y. Wang, "A multi–resolution, full–colour spatial gamut mapping algorithm," in *Proc. 11th Color Imag. Conf. IS&T/SID*, Scottsdale, AZ, USA, 2003, pp. 282–287.
[17] R. Bala, R. deQueiroz, R. Eschbach, and W. Wu, "Gamut mapping to preserve spatial luminance variations," *J. Imag. Sci. Technol.*, vol. 45, no. 5, pp. 436–443, 2001.
[18] P. Zolliker and K. Simon, "Retaining local image information in gamut mapping algorithms," *IEEE Trans. Image Process.*, vol. 16, no. 3, pp. 664–672, Mar. 2007.
[19] S. Nakauchi, S. Hatanaka, and S. Usui, "Color gamut mapping based on a perceptual image difference measure," *Color Res. Appl.*, vol. 24, no. 4, pp. 280–291, 1999.
[20] R. Kimmel, D. Shaked, M. Elad, and I. Sobel, "Space-dependent color gamut mapping: A variational approach," *IEEE Trans. Image Process.*, vol. 14, no. 6, pp. 796–803, Jun. 2005.
[21] A. Alsam and I. Farup, "Spatial colour gamut mapping by means of anisotropic diffusion," in *Computational Color Imaging*. Berlin, Germany: Springer-Verlag, 2011, pp. 113–124.
[22] P. Zolliker, Z. Barańczuk, and J. Giesen, "Image fusion for optimizing gamut mapping," in *Proc. 19th Color Imag. Conf. IS&T/SID*, San Jose, CA, USA, 2011, pp. 109–114.
[23] I. Lissner and P. Urban, "Toward a unified color space for perception-based image processing," *IEEE Trans. Image Process.*, vol. 21, no. 3, pp. 1153–1168, Mar. 2012.
[24] ICC. (2010). *File Format for Color Profiles* (4th ed.) [Online]. Available: http://www.color.org
[25] X. Zhang and B. A. Wandell, "A spatial extension of CIELAB for digital color-image reproduction," in *Soc. Inf. Display Symp. Tech. Dig.*, vol. 27. 1996, pp. 731–734.
[26] E. Reinhard, E. A. Khan, A. O. Akyüz, and G. M. Johnson, *Color Imaging: Fundamentals and Applications*. Natick, MA, USA: A K Peters, 2008.
[27] G. Johnson and M. Fairchild, "Darwinism of color image difference models," in *Proc. 9th Color Imag. Conf. IS&T/SID*, 2001, pp. 108–112.
[28] J. Giesen, E. Schuberth, K. Simon, P. Zolliker, and O. Zweifel, "Image-dependent gamut mapping as optimization problem," *IEEE Trans. Image Process.*, vol. 16, no. 10, pp. 2401–2410, Oct. 2007.
[29] F. Dugay, I. Farup, and J. Y. Hardeberg, "Perceptual evaluation of color gamut mapping algorithms," *Color Res. Appl.*, vol. 33, no. 6, pp. 470–476, 2008.
[30] Z. Barańczuk, P. Zolliker, and J. Giesen, "Image-individualized gamut mapping algorithms," *J. Imag. Sci. Technol.*, vol. 54, no. 3, pp. 030201-1–030201-7, 2010.
[31] L. Brown and X. Li, "Confidence intervals for two sample binomial distribution," *J. Stat. Plan. Inference*, vol. 130, nos. 1–2, pp. 359–375, 2005.
[32] L. Zhang, L. Zhang, X. Mou, and D. Zhang, "FSIM: A feature similarity index for image quality assessment," *IEEE Trans. Image Process.*, vol. 20, no. 8, pp. 2378–2386, Aug. 2011.
[33] Z. Wang and A. Bovik, "A universal image quality index," *IEEE Signal Process. Lett.*, vol. 9, no. 3, pp. 81–84, Mar. 2002.
[34] N. Damera-Venkata, T. Kite, W. Geisler, B. Evans, and A. Bovik, "Image quality assessment based on a degradation model," *IEEE Trans. Image Process.*, vol. 9, no. 4, pp. 636–650, Apr. 2000.
[35] D. Chandler and S. Hemami, "VSNR: A wavelet-based visual signal-to-noise ratio for natural images," *IEEE Trans. Image Process.*, vol. 16, no. 9, pp. 2284–2298, Sep. 2007.
[36] T. Mitsa and K. Varkur, "Evaluation of contrast sensitivity functions for the formulation of quality measures incorporated in halftoning algorithms," in *Proc. IEEE Int. Conf. Acoust., Speech, Signal Process.*, vol. 5. Apr. 1993, pp. 301–304.
[37] H. Sheikh, A. Bovik, and G. de Veciana, "An information fidelity criterion for image quality assessment using natural scene statistics," *IEEE Trans. Image Process.*, vol. 14, no. 12, pp. 2117–2128, Dec. 2005.
[38] N. Ponomarenko, O. Ieremeiev, V. Lukin, K. Egiazarian, L. Jin, J. Astola, *et al.*, "Color image database TID2013: Peculiarities and preliminary results," in *Proc. 4th Eur. Workshop Visual Inf. Process.*, Paris, France, Jun. 2013, pp. 1–6.
[39] Z. Wang. (2013, May 13). *SSIM* [Online]. Available: https://ece.uwaterloo.ca/∼z70wang/research/ssim/ssim.m
[40] Mattbuck. (2013, Apr. 2). *Bristol Balloon Fiesta* [Online]. Available: http://commons.wikimedia.org/wiki/File:Bristol_Balloon_Fiesta_2009_MMB_%04_G-OFXP.jpg
[41] B. Friedrich. (2013, Apr. 2). *Tropfen auf Gras* [Online]. Available: http://commons.wikimedia.org/wiki/File:Tropfen_auf_Gras_2.JPG
[42] S. Krause. (2013, Apr. 2). *S1000RR* [Online]. Available: http://commons.wikimedia.org/wiki/File:S1000RR_Composing.jpg
[43] Simple Insomnia. (2013, Apr. 2). *Berber Camel Driver* [Online]. Available: http://commons.wikimedia.org/wiki/File:S1000RR_Composing.jpg
[44] J. Morovic, "To develop a universal gamut mapping algorithm," Ph.D. dissertation, Univ. Derby, Derby, U.K., 1998.
[45] *Characterization Data for Commercial Offset Printing (ISO 12647-2:2004/Amd 1) on Gloss or Matt Coated Paper (PT 1/2) Using a Screening According to 60/cm*, Standard FOGRA27, 2003.
[46] J. Garcia. (2013, Mar. 28). *Color Balance* [Online]. Available: http://www.fotopedia.com/items/flickr-3748383024
[47] (2013, May 17). *Supplementary Material (iCID Implementation + iCID-Based Gamut-Mapping Optimization)* [Online]. Available: http://www.idd.tu-darmstadt.de/color/papers

Jens Preiss received the Diploma degree in physics from the University of Freiburg, Freiburg, Germany, in 2010. He is currently a Research Assistant with the Institute of Printing Science and Technology, Technische Universität Darmstadt, Darmstadt, Germany, where he works as a doctoral candidate in the area of color and imaging science.

Felipe Fernandes received the M.Sc. degree in mechanical and process engineering from Technische Universität Darmstadt, Germany, in 2013, and is currently pursuing the Ph.D. degree with the Institute of Printing Science and Technology. He has been a Professional Photographer since 2010.

Philipp Urban received the M.S. degree in mathematics from the University of Hamburg, Germany, in 1999, and the Ph.D. degree from the Hamburg University of Technology in 2005.

From 2006 to 2008, he was a Visiting Scientist with the Munsell Color Science Laboratory, Center for Imaging Science, Rochester Institute of Technology, Rochester, NY, USA, and the Head of the Color Research Group, Institute of Printing Science and Technology, Technische Universität Darmstadt, Darmstadt, Germany. Since 2013, he has been the Head of the Competence Center 3D Printing Technology, Fraunhofer Institute for Computer Graphics Research IGD, Darmstadt. His research interests include spectral imaging, image quality, and material appearance reproduction.